Photochemically Induced Energy Transfer II: Spectroscopic and Photophysical Aspects of the Electronic-to-Electronic Energy Transfer in Geminate van der Waals Complexes†

Robert Wagner, Frank Schouren, and Murthy S. Gudipati*

Institut für Physikalische Chemie, Universität zu Köln, Luxemburger Strasse 116, D-50939 Köln, Germany

Received: October 20, 1999; In Final Form: February 17, 2000

A detailed spectroscopic study of the *photochemically induced* electronic-to-electronic energy transfer reported by us earlier (Gudipati, M. S. *J. Phys. Chem. A* **1997**, *101*, 2003) in O···CO geminate van der Waals complexes in Ar matrices revealed that these complexes are stabilized in two distinct sites, a singly substitutional (SS) site and a doubly substitutional (DS) site. In the SS site the spectra of O and CO are strongly perturbed, whereas in the DS site spectroscopic features nearly identical to the isolated O and CO have been observed. Theoretical calculations on the ground-state O···CO complex in the SS and DS sites of the Ar lattice are in agreement with the experimental observations. Photolysis of CO_2 in Xe/CO_2/Ar matrices leads to the formation of Xe···O···CO complexes, and energy transfer from the excited CO to XeO that results in emission from XeO has been observed. Electronic spectra corresponding to the O···CO complexes in Kr matrices have also been observed, but only as weak features superposed on strong charge-transfer transitions in KrO in Kr matrices. We proposed to unify the nonresonant excitation energy transfer processes that involve the formation of an excited species under photochemically induced energy transfer.

Introduction

Excitation energy transfer (EET) is a well-known process since the beginning of atomic spectroscopy.[1] A deeper understanding of the mechanistic aspects of EET, however, has started emerging only recently.[2−4] Thus, a unified approach to represent the dipolar radiative and nonradiative EET, the latter being due to Förster,[5] is given by Andrews.[2,4] However, radiative EET (REET) involving nonconservation of spins is an exception to the unified theory presented by Andrews. An example of such REET is the reabsorption of phosphorescence of CO by a variety of aromatic molecules studied by us recently.[6,7] Recent work of Ghiggino[8] and collaborators puts some doubts on the importance of the Dexter's[9] exchange mechanism.

Though the resonant EET processes outlined above seem to be better understood, the understanding of the nonresonant EET processes has been more diffuse. Several terminologies have been used in the literature to account for this type of EET, for example: formation of excited intermediates,[10−12] nonvertical and nonspectroscopic energy transfer,[13,14] non-Franck−Condon, nonresonant and nonoptical energy transfer,[15−17] crossing of the entrance and product channels.[18] An interesting aspect of the nonresonant EET, however, is that in the majority of cases involvement of an excited complex has been postulated. We have recently observed such a nonresonant EET in (O···CO) van der Waals complex mediated through the formation of excited CO_2. In Ar matrices at 18 K, as shown in Figure 1, CO_2 is excited at 107 nm into the $^1\Sigma_u^+ \leftarrow X^1\Sigma_g^+$ transition resulting in the dissociation of CO_2 to an intracage geminate O(^{1}S) and CO($X^1\Sigma^+$) pair. O(^{1}S) relaxes to O(^{1}D) by emitting a photon at 560 nm and O(^{1}D) is deactivated to O(^{3}P) through electronic-to-vibrational energy transfer to CO.[19,20] Excitation of CO in the geminate van der Waals pair O(^{3}P)···CO($X^1\Sigma^+$) into the $A^1\Pi \leftarrow X^1\Sigma^+$ vibronic transitions between 157 and 120 nm resulted in a strong emission of O (^{1}S→^{1}D) at 560 nm. This electronic-to-electronic energy transfer could not be explained by invoking the well-known Förster−Dexter type resonant energy transfer processes. Based on the spectroscopic information and taking into consideration the excited states of CO_2 correlating to O + CO after dissociation, we named the observed energy transfer *photochemically induced* energy transfer.[21] Electronic excitation of CO in the geminate van der Waals pair results in the formation of excited CO_2, which then dissociates to CO in the ground state and O in the ^{1}S state as shown in Figure 1. The thick arrowhead line in Figure 1

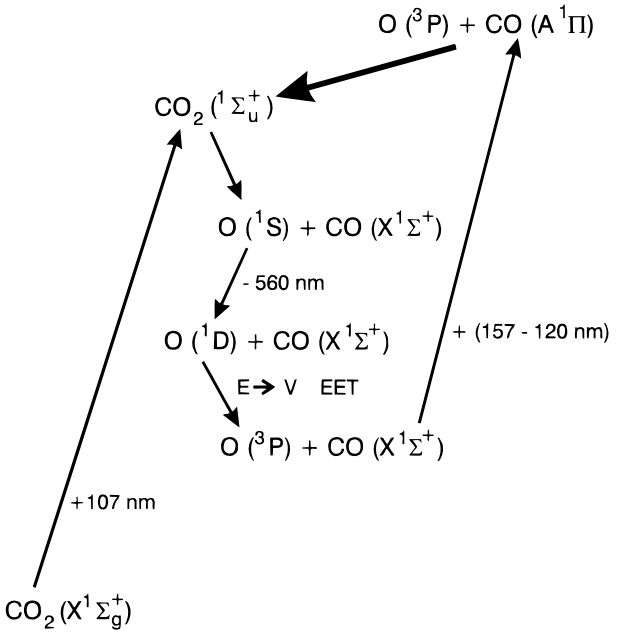

Figure 1. Schematic representation of VUV photolysis of CO_2 and the photochemically induced electronic-to-electronic energy transfer in O···CO van der Waals complexes stabilized in rare gas matrices.

† Part of the special issue "Marilyn Jacox Festschrift".

* Corresponding author. E-mail: murthy.gudipati@uni-koeln.de.

10.1021/jp993737n CCC: $19.00
Published on Web 03/30/2000

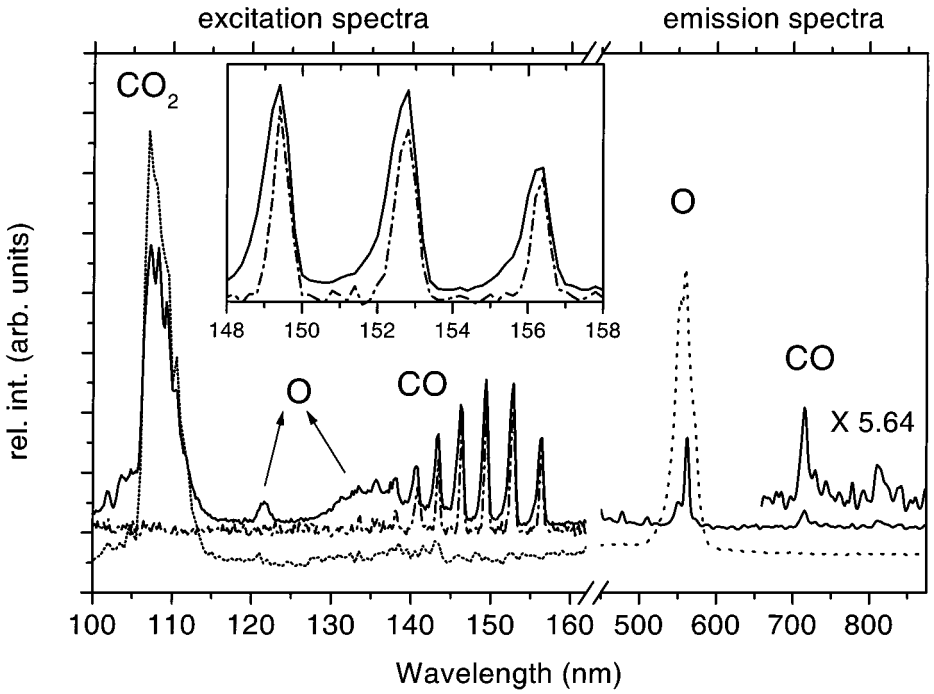

Figure 2. Excitation and emission spectra measured from 0.2% CO_2 in Ar matrices. The dotted line spectra were measured from a freshly prepared matrix (excitation at 107 nm and emission at 560 nm). Solid line spectra were recorded after partial photolysis of CO_2. The excitation spectrum was recorded by monitoring the SD emission of O atoms at 560 nm, and the emission spectrum was measured by exciting CO at 156.4 nm. The dash−dot excitation spectrum was measured from the same matrix after partial photolysis by monitoring the triplet−triplet emission of CO at 714 nm. Shown in the inset are the A←X excitation bands of isolated CO (on the 714 nm emission) as dash−dot line and CO in the O···CO complex (on the 560 nm emission) as solid line.

indicates accessing the electronic states of CO_2 by O + CO* and the internal conversion processes that occur either before or after the photochemical association of (O···CO*) to CO_2*. For example, after the $A^1\Pi \leftarrow X^1\Sigma^+$ excitation of CO, the reaction may occur immediately between $O(^3P)$ and $CO(A^1\Pi)$, or $CO(A^1\Pi)$ may relax to the lower electronic states before the reaction takes place. Similarly, CO_2* may be produced directly in the dissociative $^1\Sigma_u^+$ state or in the higher electronic states and then relax to the $^1\Sigma_u^+$ state. It is one of the aims of the present paper to track down these relaxation processes.

The nonresonant EET processes that occur through the *mutual accessing* of the electronic states of DA and D+A by each other (where D is the energy donor and A is the energy acceptor, DA can be a molecule or a complex) can thus be unified under the photochemically induced energy transfer. Parallel to the resonant EET processes, the photochemically induced EET processes can occur through the involvement of electronic, vibrational, rotational, and translational states of D and A. Further, conservation of spin is not necessary as the internal conversion processes in D* and (DA)* would dictate the final spin-states of D+A*.

In the present paper we report detailed spectroscopic and photophysical features of the O···CO system in Ar and Kr matrices. Theoretical analysis to qualitatively understand the nature of the O···CO complexes in the ground state will be presented. Results of the (Xe···O···CO) van der Waals system stabilized in Ar matrices will also be discussed.

Experimental Section

The experiments were carried out at the Berlin Synchrotron Radiation Facility (BESSY−I) using a 3 m normal incidence monochromator (3m-NIM-1). The experimental setup and other details can be found in our earlier publications.[21,22] The matrices were prepared and studied at 20 K. The guest−host ratios were 2:1000 (CO_2:Ar) and 1:2:1000 (Xe:CO_2:Ar). We had to compromise between resolution and signal-to-noise ratio with the experimental setup at hand. Thus, for the excitation spectra the resolution was 0.45 nm (fwhm), and for the emission spectra between 300 and 1400 nm the resolution was 6.3 nm (fwhm). Better spectral resolutions led to significant decrease in the signal-to-noise ratio.

Results and Discussion

Results of our previous work are summarized in Figure 2. Excitation of 0.2% CO_2 in Ar matrices at 107 nm results in a broad emission at 560 nm due to the $^1S \rightarrow {}^1D$ emission of O (here on SD emission of O). No further emission is observed between 300 and 900 nm. After partial photolysis at 107 nm, the excitation spectra measured by monitoring the SD emission of O at 560 nm contains not only the broad band at 107 nm due to the $^1\Sigma_u^+ \leftarrow X^1\Sigma_g^+$ transition of CO_2, but also the $A^1\Pi \leftarrow X^1\Sigma^+$ vibronic bands of CO between 158 and 130 nm. Additionally, the $^3S \leftarrow {}^3P$ Rydberg transition of O at 121.7 nm and the charge transfer transitions of $Ar^+O^- \leftarrow$ ArO nature between 150 and 125 nm are also seen in the excitation spectra[23] (Figure 2). Thus, photolysis of CO_2 generates not only the geminate O···CO van der Waals pair (cage confinement), but also isolated O and CO species (cage exit). Excitation at 156.4 nm into the $A^1\Pi(v' = 0) \leftarrow X^1\Sigma(v'' = 0)$ transition results in a strong SD emission of O as well as several emission bands due to triplet−triplet transitions in CO itself,[24] two of them being $a'^3\Sigma^+(v' = 6) \rightarrow a^3\Pi(v'' = 0,1)$ transitions at 714 and 815 nm, as seen in Figure 2. The excitation bands of CO are systematically broad and extend to shorter wavelengths when the SD emission of O is monitored (Figure 2 inset), whereas monitoring the triplet−triplet emission of CO at 714 nm results in relatively sharp excitation bands, identical with those recorded from only CO in Ar matrices.[21] Based on these observations we concluded

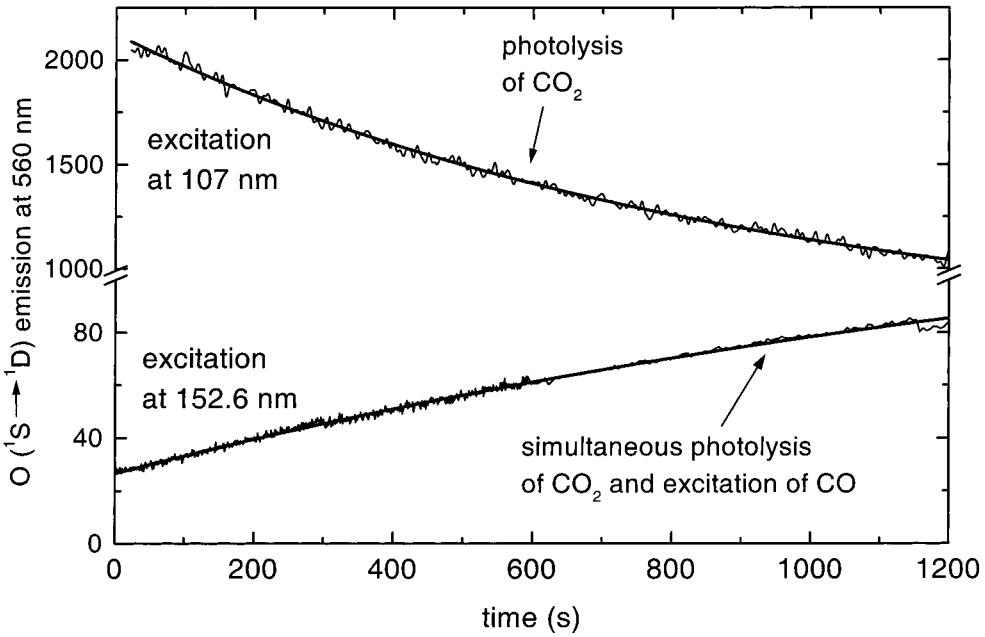

Figure 3. Changes in the SD emission intensities of O atom during the photolysis of CO_2 at two different wavelengths.

in our previous work[21] that energy transfer occurs only in the O···CO geminate van der Waals pairs and that the electronic states of CO are strongly perturbed by the presence of O. Further evidence for the formation of the van der Waals complexes comes from the fact that the energy transfer from CO to O is observed only when CO_2 is photolyzed in Ar matrices, not when O atoms are formed from O_2 in Ar matrices containing O_2 and CO.[21] Photolysis of CO_2 at 107 nm results in direct production of O(^{1}S), whereas at longer wavelengths O(^{1}D) is produced, which relaxes to O(^{3}P). Thus, the SD emission of O decreases with time of photolysis at 107 nm as shown in Figure 3. When photolyzed at 152.6 nm, where CO_2 absorbs weakly but at which wavelength CO has strong absorption due to the $A^1\Pi(v' = 1) \leftarrow X^1\Sigma^+(v'' = 0)$ transition, a steady increase in the SD emission of O is observed (Figure 3). Both of the curves in Figure 3 can be fitted to a monoexponential photolysis of CO_2. These data further confirm that photolysis of CO_2 results in the formation of *intracage geminate van der Waals complexes* of O···CO that participate in the photochemically induced energy transfer.

Nature of the Broad Excitation Bands of CO. To get further insight into the nature of the geminate complexes and broadening of the CO excitation bands shown in the inset of Figure 2, we have carried out detailed spectroscopic studies. We chose to look at the first three vibronic bands of the CO A←X transition at 156.4, 152.8, and 149.6 nm, as the rest of the bands overlap with the charge transfer bands of ArO[23] (Figure 2). By exciting at different positions of these three bands emission spectra were recorded between 530 and 580 nm, which are shown in Figure 4a. It is immediately evident that excitation at a shorter wavelength shoulder of each band results in a broad emission between 540 and 570 nm, whereas excitation at the band maxima results in a relatively sharp emission band between 555 and 570 nm with a shoulder at 550 nm. These spectra reveal that the broad excitation bands of CO are not due to a single but rather to two distinct sites of Ar lattice in which the O··· CO geminate complexes are located. Excitation spectra recorded by monitoring the emission at 551 and 562 nm are shown in Figure 4b. When the emission at 551 nm is monitored, the excitation bands are indeed shifted to shorter wavelengths, exactly covering the regions of the shoulders of the excitation

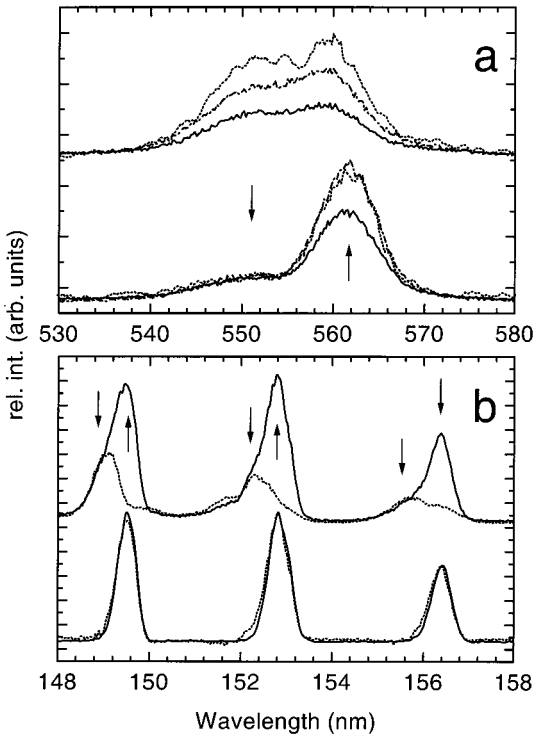

Figure 4. (a) Resolved SD emission of O measured by exciting CO at different wavelengths. The upper set of spectra were recorded by exciting at shorter wavelength side and the lower set of spectra were measured by exciting at the maximum of each vibronic band of CO shown in the part (b). The excitation wavelengths are indicated with arrowhead lines. (b) Excitation spectra of CO measured by monitoring different regions of the SD emission of O as marked with arrowhead lines in the part (a). For the dotted line excitation spectrum the emission was monitored at 551 nm. In the lower part, the spectrum derived by subtracting the dotted line spectrum from the solid line spectrum, shown as dotted line spectrum, is compared with the excitation spectrum of isolated CO.

bands obtained by monitoring the emission at 562 nm. This further indicates that excitation into the shorter wavelength bands results in emission of approximately equal intensities at 551 and 562 nm. After subtracting the excitation spectrum corre-

sponding to the emission at 551 nm from that corresponding to the emission at 562 nm, the resulting spectrum is nearly identical to the excitation spectrum of CO recorded by monitoring the a′(v=6)→a(v=0) emission of CO at 714 nm (Figure 4b lower part). Thus, the broad excitation bands of CO are due to two sites in which O···CO geminate complexes find themselves, of which in one site the electronic states of CO as well as O are strongly perturbed and in the other site both CO and O behave spectroscopically as if they were isolated. It is well documented in the literature that in Ar matrices CO_2 occupies two distinct sites with equal probability, namely, singly substitutional (SS) by replacing one Ar atom and doubly substitutional (DS) by replacing two Ar atoms.[25,26] In our earlier work we assumed that the O···CO geminate complexes are formed only in the SS site, whereas in the DS site, due to more cavity volume, O···CO recombination to CO_2 in the $^3B_2$ state occurs. Our new data given in Figure 4 shows that this assumption is wrong and the geminate O···CO van der Waals pairs are generated during the photolysis of CO_2 in both SS and DS sites. In the SS site, due to less cavity volume, the spectroscopic properties of both O and CO are strongly perturbed. In the DS, the cavity volume is large enough for the O···CO pair to relax so that their spectroscopic properties are nearly identical to isolated O and CO in Ar matrices. Broad and blue-shifted SD emission of O from the O···CO geminate pair in the SS site is reminiscent of the same emission of O in the tight interstitial site of Ar lattice.[23] Similarly, the sharp 562 nm emission of O from the O···CO geminate pair in the DS site resembles highly the SD emission of O from a substitutional site.[23] Thus the above assignment of the two sites of O···CO to SS and DS sites is further justified.

Spectroscopic Features of the O···CO Complex in the SS Site. Due to the identical spectroscopic features of O and CO in the O···CO complex in the DS site with the respective isolated O and CO, under steady-state conditions that are employed in the present study, it is not possible to get further information on the O···CO complex in the DS site. For this reason we discuss the spectroscopic features of the O···CO complex and the details of the energy transfer in the SS site and assume that in the DS site similar processes occur. We have measured in detail the excitation and emission spectra of the O···CO complex in the SS site involving the three CO excitation bands between 157.5 and 148 nm (Figure 4). The properties discussed below are identical for all the three excitation bands, and hence only the spectra from one of these bands are shown in Figure 5. In Figure 5a the 0−0 region of the A←X excitation is shown, in Figure 5b the Cameron emission region is presented, and in Figure 5c the SD emission of O is given.

It would be helpful to briefly touch upon the relaxation processes in electronically excited CO in Ar matrices for the discussion of the contents of Figure 5 and the following. A part of the electronic states of CO and the excitation and emission spectra between 120 and 1500 nm are shown in Figure 6. After the initial excitation into the A←X vibronic bands between 157 and 120 nm, very weak direct A→X VUV emission and an efficient intersystem crossing to the vibrationally excited triplet states occur in less than 10 ps.[27] Further relaxation of the excited CO occurs through a cascading process over the vibronic levels of the triplet states e, d, a′, and a (Figure 6). At bottlenecks, where the neighboring vibrational levels of different electronic states are largely separated from each other, radiative relaxation occurs from the higher triplet states (e, d, and a′) to the a and X states with lifetimes of the order of 10 to 100 ns.[27,28] The e, d, and a′ → a triplet−triplet emission occurs in the visible to infrared region (Figure 6). It is necessary to excite higher

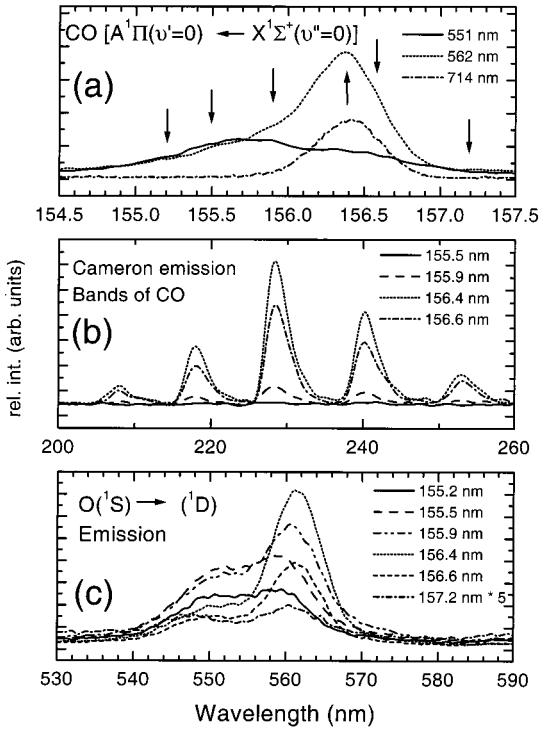

Figure 5. The 0−0 region of the A←X excitation spectrum of CO (part a), the a→X Cameron emission bands of CO (part b) and the SD emission of O (part c). The respective excitation and emission wavelengths are also listed in the figure.

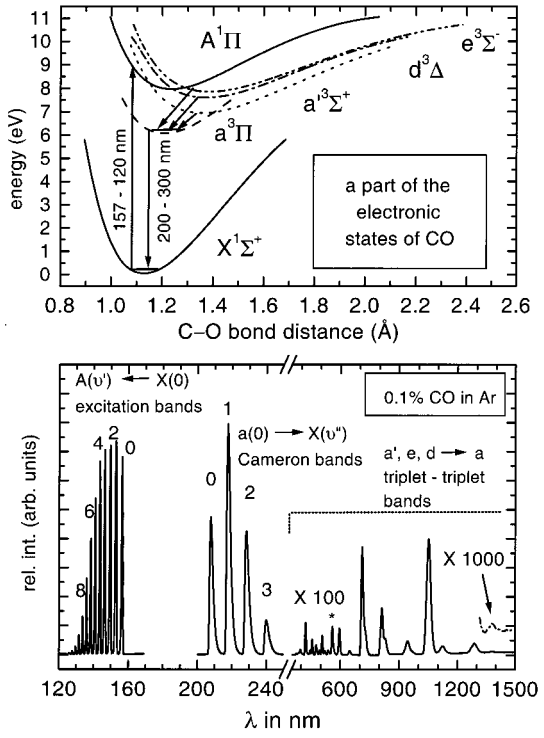

Figure 6. A part of the electronic states of CO (top part) and the excitation and emission spectra of CO in Ar matrices (bottom part). Note that the triplet−triplet emission between 350 and 1500 nm occurs before the Cameron emission between 200 and 250 nm.

vibrational levels of the A state in order to observe the triplet−triplet emission between 400 and 600 nm. Emission at longer wavelengths can be observed by exciting into the 0-vibrational level of the A state as well. In the gas phase this triplet−triplet emission is observed down to 2850 nm.[29] In Ar matrices we recorded this emission between 350 and 1500 nm as shown in

Figure 6.[24] After final cascading to the $a^3\Pi(v = 0)$ state, CO undergoes radiative relaxation to the ground state with quantum yields near to unity due to the fact that the spin−orbit coupling between the a state and the X state is negligible.[30] The radiative lifetime of the $a^3\Pi(v = 0)$ state measured from the a→X emission between 200 and 300 nm, also known as the Cameron emission, is 7.2 ms in Ar matrices.[31] Two important aspects can be derived from the above discussion. After excitation of CO into the A state at first the visible and infrared triplet−triplet emission occurs at longer wavelengths than 400 nm and then the Cameron emission between 200 and 300 nm. Lifetime of the excited CO is at the maximum 100 ns in the upper triplet states, whereas the $a^3\Pi(v = 0)$ state is a metastable state with 7.2 ms radiative lifetime in Ar matrices.

Now we shall analyze the data given in Figure 5. As the excitation wavelength is scanned over the 0−0 band of the A←X transition from the longer to the shorter wavelengths, one observes that Cameron emission bands disappear completely when excited at 155.5 nm where isolated CO no longer absorbs (compare to the excitation band corresponding to the emission at 714 nm in Figure 5a). On the other hand, excitation at this wavelength results in maximum intensity of the broad SD emission of O as can be seen in Figure 5c. Thus, the photochemical association of O···CO* to CO_2* occurs at least then, when the excited CO reaches the zero vibrational level of the $a^3\Pi$ state. Further, the absence of the Cameron emission from the SS site clearly demonstrates the nonradiative nature of the energy transfer. As mentioned earlier, the spectra of O and CO in the DS site are indistinguishable from those of isolated O and CO. However, based on the behavior of O··· CO in the SS site, we assume that in the DS site a similar process occurs, that is, the photochemical association of the complexes occurs either from the $a^3\Pi(v = 0)$ state or from the other states that lie energetically higher than this state and the energy transfer is nonradiative.

The consequence of strong perturbation of the electronic states of CO in the SS site can also be seen in the broad nature of the CO excitation bands as well as the SD emission of O. A surprising aspect of these spectra is that even when excited at 157.2 nm, at the longer wavelength side of the 0−0 band of the A state where isolated CO does not absorb any longer, SD emission of O from the O···CO pair in the SS site can clearly be observed (Figure 5c). The extreme broadening of the CO excitation bands in the SS site of the complex may be due to van der Waals vibrations of the O···CO complex as well as to the coupling of phonons of the Ar lattice with the van der Waals and electronic states of the complex. Fitting Gaussian curves on the 0−0 and 1−0 bands of the A←X transition gives two bands with a separation of around 300 cm^{-1}. The 2−0 band does not show any substructure (Figure 4). Similarly fitting Gaussian curves to the broad, but clearly observable double maxima of the SD-emission of O of the complex in the SS site gives the same separation of around 300 cm^{-1}. Based on these observations we tentatively assign these features in the excitation and emission spectra to O···CO van der Waals vibrations. Another possible explanation to the observed structure in the excitation and emission spectra of O···CO in the SS site is that, due to the tight cavity volume in the SS site, the O···Ar distances lie in a region where ArO electronic states already emerge, thus splitting the atomic states of Ar and O to molecular states of ArO.[32,33] The electronic excitation is then no longer localized in CO molecule alone, but it is delocalized in the Ar_n···O··· CO van der Waals complex in the SS site. Measurements with better spectral resolution are necessary in order to get more accurate data on the nature of the broadening of the emission and excitation spectra of O···CO in the SS site of the Ar lattice.

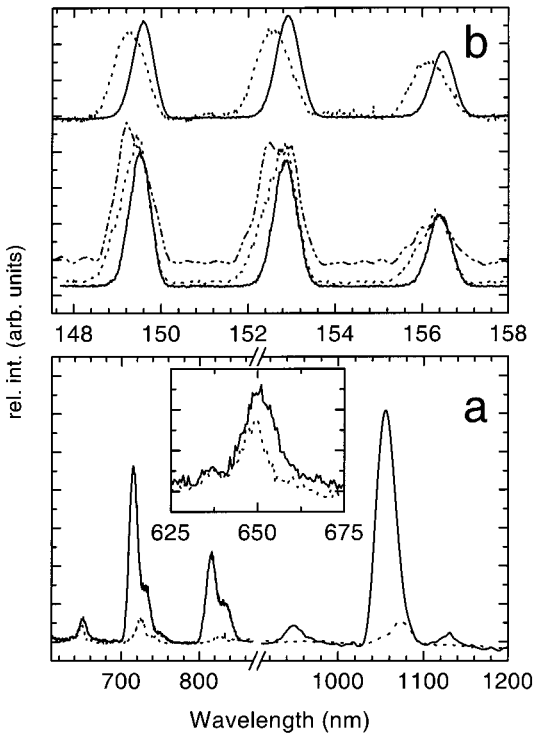

Figure 7. (a) triplet−triplet emission bands of CO recorded by exciting into the $A(v' = 1) \leftarrow X(v'' = 0)$ transition at 152.8 nm (solid line spectrum) and 152.2 nm (dotted line spectrum). In the inset, the 648 nm emission region is expanded. (b) A ← X excitation bands of CO recorded by monitoring the emission from isolated CO (solid line spectra) and from CO in the O···CO complex (dotted line spectra). To guide the eye, the dotted line spectra are scaled up in intensity to match the solid line spectra. The top two spectra were recorded by monitoring the CO emission at 1055 and 1075 nm, respectively. In the bottom part, a slightly vertically displaced spectrum was measured by monitoring the emission at 648 nm. The other two spectra were recorded by monitoring the emission at 714 and 724 nm, respectively.

We know that excited CO goes through radiative and nonradiative relaxation in the triplet manifold before reaching the lowest triplet state. Thus, the triplet−triplet emission channels should give us further information on whether the photochemical association of the O···CO complex occurs before reaching the $a^3\Pi$ state or not. For this reason we have measured the emission spectra between 600 and 1200 nm by exciting CO in the SS and DS sites. These spectra are shown in Figure 7. Unlike the Cameron bands that completely disappear when CO in the SS site is excited, one observes weak and red-shifted emission of CO from the complex in the SS site. For example, the 714 nm emission of the isolated CO is shifted to 724 nm and the 1055 nm band is shifted to 1075 nm. An exception to this trend is the band around 650 nm. Excitation of CO in the SS site results in a blue-shifted and, compared to the other bands, strong emission at 648 nm. This emission could be due to the $^1D \rightarrow {}^3P$ emission of O in the O···CO complex in the SS site. The excitation spectra that were measured by monitoring the emission at 648, 724, and 1075 nm show the same broad and blue-shifted character of the CO A←X vibronic bands as shown in Figure 7b (compare to the inset in Figure 2). Due to the weak nature of the triplet−triplet emission that is 2 orders of magnitude weaker than the Cameron emission, we had to forego the resolution to improve the signal-to-noise ratio. Thus, the fine structure seen in Figures 4 and 5 is not observed in Figure 7. As the emission at 714 (724) nm occurs from a higher

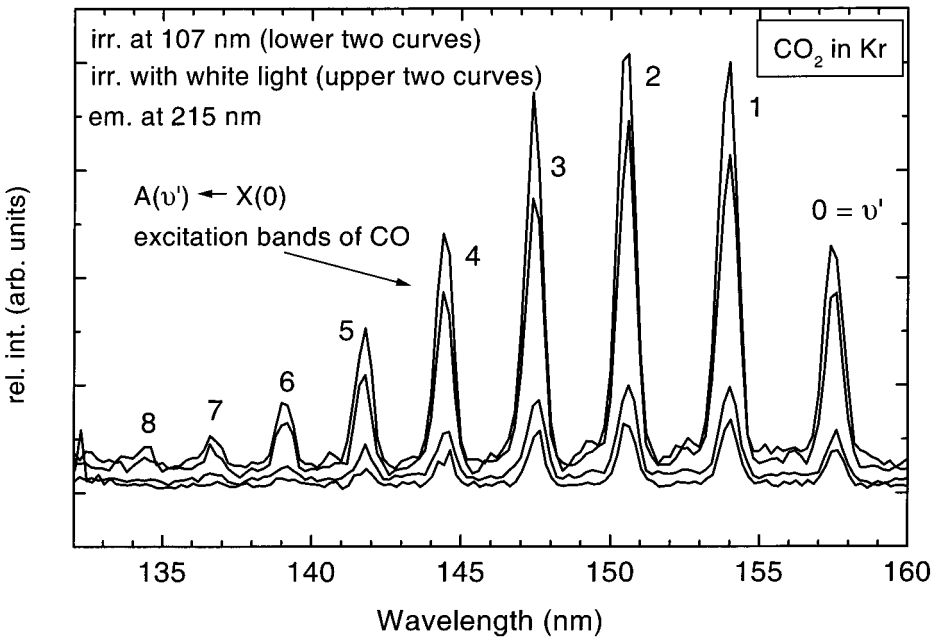

Figure 8. A(v') ← X(0) vibronic excitation bands of CO that is generated during the photolysis of CO_2 in Kr matrices.

vibrational state than the emission at 1055 (1075 nm), the intensities of these two sets of bands may give further information whether the photochemistry occurs during the relaxation of CO in the triplet manifold or not. Thus, if the photochemical channel competes with the internal relaxation in CO, then fewer CO molecules should emit at 1075 nm than at 724 nm. As we measured the two regions of the spectra with two different detectors, we have taken the ratio between 1055 and 714 nm bands and compared with the ratio between the 1075 and 724 nm bands after integration. These ratios were calculated from the emission spectra measured by exciting CO into the first three vibronic bands. Thus, by exciting into the 0−0, 1−0, and 2−0 bands of isolated CO the 1055 nm/714 nm intensity ratios are 2.5, 2.65, and 2.4, respectively. Excitation of CO in the SS site at respective shorter wavelength results in the 1075 nm/724 nm intensity ratios of 2.2, 1.9, and 2.1. Thus, there is a tendency that the 1075 nm emission is somewhat weaker than the 724 nm emission of CO in the SS site, indicating that the photochemical association may be competing with the electronic relaxation in CO in the manifold of triplet excited states.

Photolysis of CO_2 in Kr Matrices. To investigate whether the O···CO complexes also behave similar in Kr matrices or not, we carried out experiments on 0.2% CO_2 in Kr. An important difference between Ar and Kr matrices is that the first excitonic absorption of Ar crystals lies at shorter wavelength (105 nm) than the Kr excitonic absorption (125 nm) and we may note that the $^1\Sigma_u^+ \leftarrow X^1\Sigma_g^+$ excitation of CO_2 lies at 107 nm. For this reason Ar matrices are transparent at 107 nm and the photolysis of CO_2 can be achieved efficiently throughout the bulk of the matrices. However, in Kr matrices the photolysis of CO_2 at 107 nm is governed by the penetration depth of the light at this wavelength into the Kr crystals. Thus, one would expect only a partial photolysis of CO_2 at 107 nm. On the other hand, as CO_2 can be photolyzed at longer wavelengths (for example 152.6 nm as shown in Figure 2), though less efficiently, using the 0^{th} order white light of the synchrotron radiation having all the wavelengths of the light, photolysis of CO_2 can also be achieved throughout the bulk of the Kr matrices. We have followed the photolysis of CO_2 by measuring the A←X vibronic bands of CO monitoring the a→X Cameron emission at 215 nm. These spectra shown in Figure 8 reveal that CO_2 is indeed

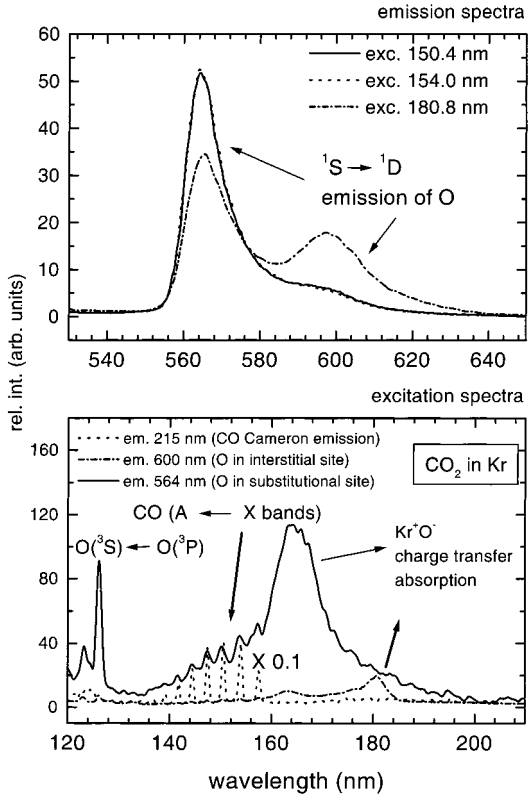

Figure 9. Emission (upper part) and excitation (lower part) spectra of O and O···CO complexes in Kr matrices. The respective excitation and emission wavelengths are also listed in the figure.

photolyzed efficiently in Kr matrices generating CO. We have also followed the production of O atoms through the excitation spectra of O in Kr by monitoring the SD emission of O at 564 and 600 nm,[23,34] in agreement with the production of CO. Surprisingly, these excitation spectra recorded by monitoring the SD emission of O are dominated by the charge transfer and Rydberg excitation of O in Kr matrices. The A←X vibronic bands of CO are barely seen as shoulder progressions on the CT excitation band as shown in Figure 9. Comparing Figure 9 with Figure 2 demonstrates that in Ar matrices the CO vibronic

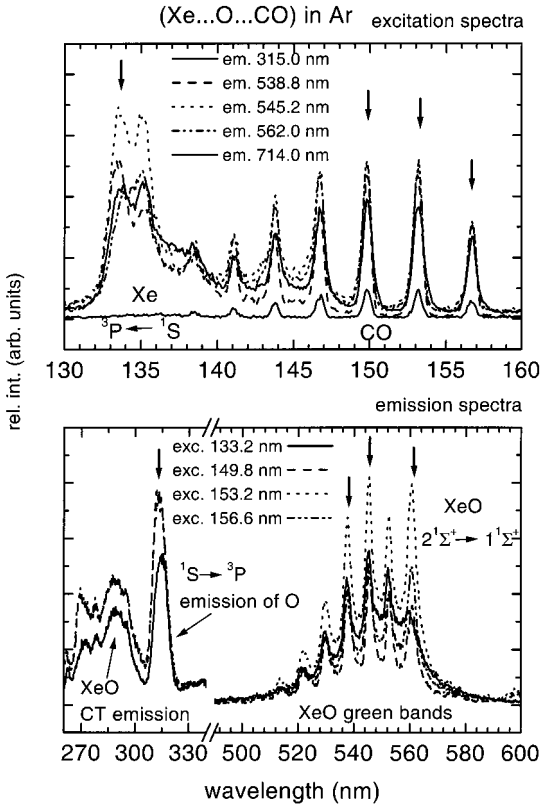

Figure 10. Excitation (top part) and emission (bottom part) spectra of Xe···O···CO van der Waals complexes generated through photolysis of CO_2 in $Xe/CO_2/Ar$ matrices. For comparison the excitation spectrum of isolated CO from the same matrix by monitoring the triplet−triplet emission at 714 nm is also included in the top part. Otherwise, the excitation and emission wavelengths used to record the corresponding spectra are also listed in the figure.

bands dominate the excitation spectrum due to efficient EET from CO to O, but in Kr matrices the spectra of isolated CO and O species dominate the excitation spectra. We believe that the cage confinement of O and CO during the photolysis of CO_2 in Ar matrices is more efficient than in Kr matrices. O atoms may exit the mother cage most likely in their ^1D state due to their smaller size[35] and due to attractive interactions between $O(^1D)$ and $Kr(^1S)$ atoms. Thus, the role of matrix material is an important factor to be considered for the photochemical generation of van der Waals complexes and to study their interactions in rare gas matrices.

Energy Transfer in Xe···O···CO van der Waals Complexes. In the previous sections we have seen that the cavity volume, whether in the tight SS or rather loose DS sites of Ar lattice, does not influence the EET in the O···CO complexes, but does influence the spectral features of O and CO. What would happen if we force an increase of the cavity volume by introducing larger atoms such as Xe? Does the Ar cage still confine and stabilize the O···CO van der Waals complexes, now including Xe, namely, Xe···O···CO? Or do O and CO recombine efficiently to bent CO_2 in the $^3B_2$ state and subsequently to CO_2 in the ground state? To answer these questions we carried out investigations on $Xe/CO_2/Ar$ matrices at different dilutions (1:2:200, 1:2:500, and 1:2:1000). The excitation and emission spectra of matrices (1:2:200 of $Xe/CO_2/Ar$) recorded after photolyzing CO_2 at 107 nm are shown in Figure 10. At higher dilutions the corresponding spectra became weaker in intensity due to the statistical nature of formation of the Xe/CO_2 complexes, but their spectral features did not change.

As can be seen in Figure 10, we indeed observe a very efficient EET from excited CO to XeO. By exciting CO into the A←X vibronic bands we could measure the CT emission at 289 nm, the $^1S \rightarrow {}^3P$ emission of O at 315 nm, and the $2^1\Sigma^+ \rightarrow 1^1\Sigma^+$ green bands of XeO starting from around 500 nm and converging with the 560 nm band.[36,37] If we qualitatively take the sum of the intensities of the UV and green emission bands of XeO and compare with the 560 nm SD emission of O, in the Xe···O···CO and O···CO van der Waals complexes, respectively, then the efficiency of energy transfer is at least an order of magnitude greater in the Xe···O···CO complex than in the O···CO complex. The line widths of the A←X excitation bands of CO, which result in the emission from isolated CO at 714 nm or from XeO at 537.4 and 545.4 nm or from O at 560 nm, are all nearly identical as shown in Figure 11. This is only

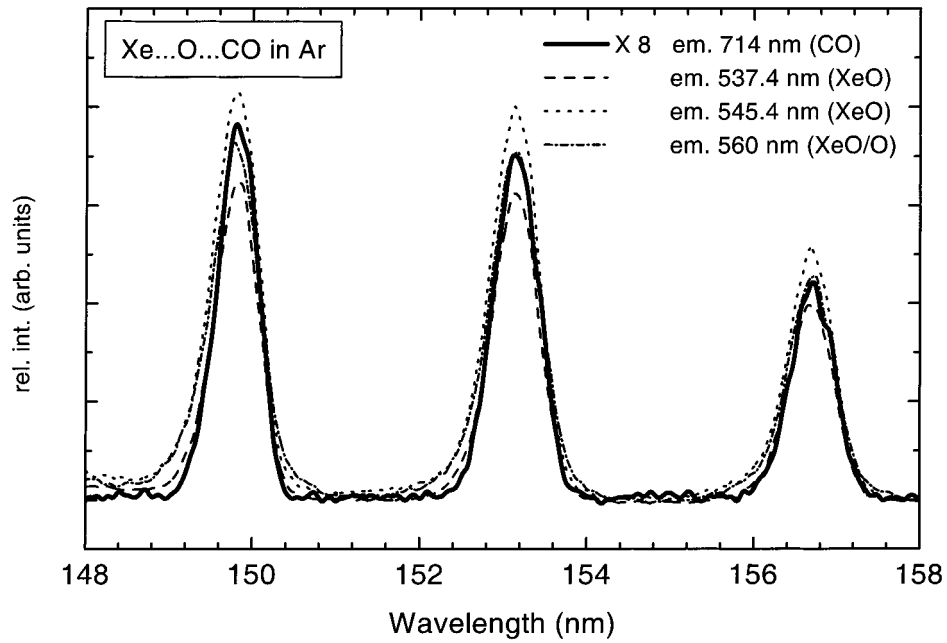

Figure 11. Comparison of the first three vibronic bands of A ← X excitation measured by monitoring different emission wavelengths as indicated in the figure. Nearly identical bandwidths indicate that CO in the Xe···O···CO complex behaves similar to an isolated CO.

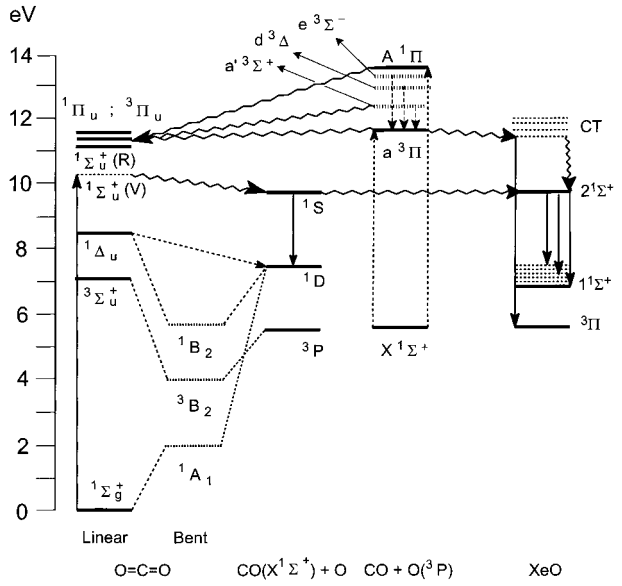

Figure 12. Schematic representation of possible relaxation, photochemical association, and energy transfer pathways in the Xe···O··· CO van der Waals complex.

possible when the O···CO part of the Xe···O···CO complex occupies a DS site of the Ar lattice and the Xe atom replaces one more Ar atom, leading to a triply substitutional (TS) site in the Ar lattice. Otherwise, similar to O···CO in SS site, the spectral features of Xe···O···CO must have been different from those of isolated CO and isolated XeO[37] in Ar matrices.

Due to the fact that we observe the CT emission of XeO at 289 nm, energy transfer from excited CO must occur into the CT states of XeO. Recent theoretical work[38] on the CT-states of XeO as well as our unpublished theoretical and experimental results[39] reveal several triplet and singlet CT states of XeO around 6 eV. Thus, an exchange-type energy transfer: $CO(a^3\Pi) + XeO(X^3\Pi) \rightarrow CO(X^1\Sigma^+) + XeO(^1\Pi,^1\Sigma - CT)$ is one of the possible pathways. However, we cannot rule out the possibility of the formation of the XeOCO molecule in its excited state, which then dissociates to XeO (CT) + $CO(X^1\Sigma^+)$. Population of the $XeO(2^1\Sigma^+)$ state that relaxes radiatively to the $XeO(1^1\Sigma^+)$ state by emitting photons between 500 and 560 nm (Figure 10) may have two different pathways. The first one is the relaxation of the XeO(CT) to the $XeO(2^1\Sigma^+)$ and the second one is through the photochemical pathway of the O···CO complex leading to $O(^1S)$, which then reacts with $Xe(^1S)$ resulting in the $XeO(2^1\Sigma^+)$. These different radiative and nonradiative relaxation pathways in Xe···O···CO are schematically shown in Figure 12. Time-resolved measurements are needed to be carried out to get further insight into the complex pathways of EET in this system.

Theoretical Calculations on the Ground State O···CO van der Waals Complex in the SS and DS Sites. In the preceding sections we have seen that the O···CO van der Waals complexes show different spectroscopic signature in the SS and DS sites in Ar matrices as well as in the presence of Xe in Ar matrices. Ideally, if one could have at least the three-dimensional potential energy surfaces of all of the relevant electronic states of O··· CO correlating to CO_2, then one could get precise information on how this photochemically induced energy transfer occurs in the O···CO complexes in different environments. To achieve this it is necessary to carry out highly reliable ab initio calculations that deliver the potential energy surfaces with an accuracy of the order of a few meV, especially at regions of weak interactions (large O···CO separations). Unfortunately, there exist only a few theoretical publications on the potential energy curves of CO_2 dissociating to O + CO[40,41] or C + O_2,[40] involving only the first two electronic states of O (^3P and ^1D) and the ground-state of CO ($X^1\Sigma^+$). As a first step toward achieving this goal we carried out theoretical investigations on the nature of the ground-state $O(^3P) + CO(X^1\Sigma^+)$ van der Waals complexes in the SS and DS sites of Ar lattice. Earlier experimental work of Clyne and Thrush[42] in the gas phase gives an activation barrier of about 3.7 ± 0.5 kcal/mol (0.16 ± 0.02 eV) for the $O(^3P) + CO(X^1\Sigma^+) \rightarrow CO_2(^3B_2)$ reaction. Recent theoretical work[41] at the MP2 level shows a barrier for this reaction, with no details on the nature of the barrier. These calculations were done using 6-31G* basis set and only a partial scan of the two-dimensional potential energy surface was carried out by these authors. For this reason we have undertaken a detailed computation of the potential energy surfaces of the O···CO complex in the gas phase and in the Ar lattice. As we are dealing with O···CO complexes in Ar lattices, we need to compute the potential energy of interactions between the guest O···CO complex and host Ar lattice. We call the contribution from the host−guest interactions as the external potential energy and the gas-phase energy as the internal potential energy. Summing up these two contributions at a given O···CO geometry then gives the total energy of the complex in the Ar lattice.

The internal potential energy surface of the triplet ground-state O···CO complex correlating to the lowest triplet state of CO_2 was computed by a relaxed PES scan with the MP2-method implemented in the *Gaussian 98*[43] program. The oxygen atom was moved on a quarter circle around the carbon atom of the CO fragment, varying the O···C−O angle "α" between 90° and 180° in steps of 10°, while the O···CO distance "*R*" was varied from 1.1 to 3.6 Å in steps of 0.1 Å, leading to a total of 260 points on the PES. After calculating the energy at a given *R* and α, for an initial guess of the C−O bond length "*r*", a new single point calculation was started allowing the parameter *r* to be optimized. This relaxed PES scan was continued at each point until convergence. To properly describe the long-range interactions that are apparent in the investigated system, it is essential to employ basis sets of sufficient diffuseness. For reasons of comparison the calculations were carried out with four different basis sets ranging from medium sized to large ones (6-31G*, aug-cc-pVDZ, cc-pVTZ, aug-cc-pVTZ). All calculations show a van der Waals minimum at a linear O···CO geometry. For the calculations employing the aug-cc-pVTZ basis set, the depth of this minimum is 20.3 meV and the distances *r* and *R* are 1.139 and 3.2 Å, respectively. Otherwise the potential curve at linear geometry is strictly repulsive, as are those at 170° and 160°. Beginning at an O···CO angle of 150°, a potential barrier at *R* around 1.7 Å is formed. The global minimum of the $^3B_2$ state of CO_2 and the barrier minimum (first-order saddle point) is found at α around 120°. The geometries and the energies of O···CO at the saddle point and at the minimum computed using the above-mentioned four basis sets are given in Table 1. One can see that increasing the size of the basis set leads to an increase in the binding energy and a decrease in the barrier energy. On the other hand, the basis set dependence of the corresponding geometrical parameters is negligible. Thus we may expect further lowering of the barrier when higher level computations are carried out, and hence the discussion of the present ab initio data should be limited to qualitative purposes with respect to the energy. The gas-phase potential energy surface of O···CO using aug-cc-pVTZ basis set is shown in Figure 13.

The external potential energy is computed as follows. Initially an O···CO pair of a given geometry was positioned with its

TABLE 1: MP2 Level Ab Initio Geometries and Energies of the O···CO Complex Correlating to the $^3B_2$ State of CO_2 at the Energy Minimum and at the Saddle Point

	minimum				saddle point			
basis set	r (Å)	R (Å)	α (°)	E (eV)	r (Å)	R (Å)	α (°)	E (eV)
6-31G*	1.195	1.327	121.09	−0.433	1.155	1.810	121.74	0.543
6-31G*[a]	1.194	1.325	121.1	−0.78[b]				0.4−0.6[c]
aug-cc-pVDZ	1.195	1.331	121.47	−0.437	1.154	1.818	122.46	0.506
cc-pVTZ	1.187	1.311	121.29	−0.588	1.142	1.825	121.63	0.498
aug-cc-pVTZ	1.188	1.311	121.20	−0.637	1.142	1.831	121.97	0.453

[a] From the literature (ref 41). [b] There is a discrepancy between the listed and graphically represented energies in ref 41. [c] Extracted from the graph in ref 41.

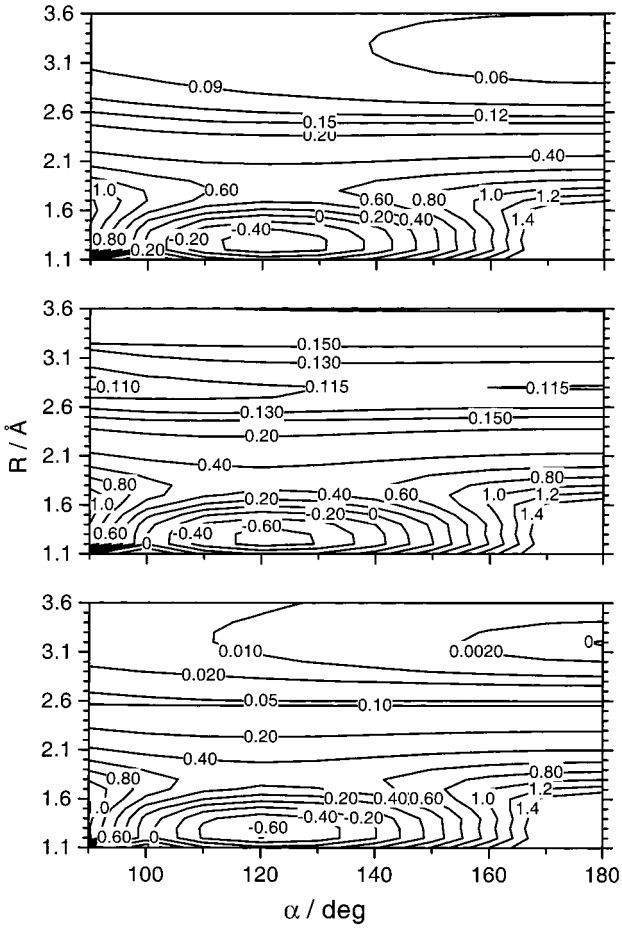

Figure 13. Contour plots of the PES of ground state O···CO complex correlating to the $^3B_2$ state of CO_2 in the gas phase (bottom) and in the SS (middle) and DS (top) sites of Ar lattice. The energy scale is in eV. Below 2.6 Å of *R* values the contours are drawn at 0.2 eV intervals. Between 2.6 and 3.6 Å of *R* the contour scale is expanded accordingly to show the van der Waals minima.

center of mass at the origin of a single (SS) respectively double (DS) vacancy of an otherwise perfect fcc argon crystal (lattice constant 5.311 Å). A cluster size of 554 Ar atoms (SS site, 19 shells) or 544 Ar atoms (DS site, 40 shells) was employed. A shell is defined as the cluster containing equidistant Ar atoms from the center of the cavity where O···CO is placed. The energy of these Ar clusters containing O···CO as impurity was calculated using the atom−atom approximation,[44,45] i.e., summing up all individual Ar···Ar, Ar···O, and Ar···C pair potentials. We used the (6-exp) Buckingham form and potential parameters given in a recent publication.[46] The energy difference between clusters containing the O···CO complex and the undistorted lattice without any defects, i.e., pure Ar clusters containing 554+1 atoms (SS site) or 544+2 atoms (DS site) was computed. For each geometry of the O···CO complex this energy difference, also known as solvation energy of the impurity,[47] was minimized using the conjugate gradient (CG) method (Polak−Ribiere prescription).[48] In this search of the optimal geometric configuration of the whole cluster, the center of mass of the O···CO van der Waals pair, three orientation angles, which allow rotation of the O···CO pair around the *x*, *y*, and *z* axes, and the coordinates of Ar atoms building the first three shells (SS site, 42 Ar atoms) respectively the first six shells (DS site, 38 Ar atoms) were allowed to relax. Thus, computed potential energies at each O···CO geometry were then added to the gas-phase energies. The resulting three-dimensional potential energy surfaces for O···CO in the SS and in the DS sites are shown in Figure 13 as contour plots.

We see close resemblance between the gas-phase PES and the PES in the DS site in Ar lattice of O···CO. In both the cases the energy minimum is at around 3.2 Å of *R*. In the DS site the saddle point is located at $R = 1.8$ Å and $\alpha = 120°$ and the barrier of 0.49 eV in the DS is nominally higher than that in the gas phase (0.45 eV). Thus, the theoretical computations predict O and CO in the ground state of the O···CO complex in the DS site to behave like the respective isolated species, which is in excellent agreement with the experimental results. On the other hand, in the SS site, the PES of O···CO has a different signature than the PES in the DS site and in the gas phase. We find steeper PES with respect to *R*, the minimum being at $R = 2.8$ Å, but an almost isoenergetic region for the angle α between 90° and 180° (Figure 13). Thus, in the SS site the O···CO distance, *R*, is shortened by 0.4 Å compared to the gas-phase van der Waals distance due to the compact cavity of the SS site. Thus, one would expect strong perturbation of the spectroscopic properties of O and CO in the O···CO complex in the SS site, again in agreement with the experimental results discussed in the preceding sections. Similar to the gas phase and in the DS site, the saddle point in the SS site is located at $R = 1.8$ Å and $\alpha = 120°$. However, the barrier for the reaction from the energy minimum is 0.34 eV, lower by 0.11 eV than in the gas phase and in the DS site. We have mentioned earlier that at MP2 level of ab initio computations using different basis sets (Table 1), though the geometrical parameters have converged, the energies of the saddle point and the minimum in the PES have not yet converged. If we assume that the gas-phase experimental barrier derived by Clyne and Thrush[42] from the measurements at temperatures between 198 and 284 K is the minimum limit, namely, 0.16 ± 0.02 eV, then in the SS site the barrier for the recombination of the ground-state O··· CO complex takes a minimum value of 0.05 ± 0.02 eV. This barrier is still far too high for the recombination reaction at 20 K. We have warmed the matrices up to 25 and 28 K to find out whether the O···CO complexes in the SS site selectively disappear by overcoming the reaction barrier to form CO_2 in its $^3B_2$ state. In both the cases no selective diminution of the spectral intensities corresponding to the O···CO in the SS site were

observed, indicating that the barrier of reaction is much higher than the thermally accessible energy at these temperatures.

In conclusion, theoretical computations predict the spectroscopic signature of O and CO in the O···CO complex to be similar to that of isolated O and CO in the DS site and to be strongly perturbed in the SS site of the Ar lattice, in agreement with the experimental observations. Due to the nonconvergence of the energies with different basis sets used at the MP2 level, it is likely that the theoretically obtained gas-phase reaction barrier, and hence the reaction barrier in the Ar lattice, is over estimated. Higher level ab initio computations at CASSCF or CCSDT levels with even larger basis sets may give more reliable PES.

Conclusions

In the present contribution we have proposed to unify energy transfer processes that occur through the formation of excited species under photochemically induced energy transfer processes. In the case of O···CO van der Waals complexes generated in Ar matrices, it has been shown that these complexes are stabilized by the host lattice in both SS and DS sites. The spectroscopic signature of the O···CO complex in both of these sites has clearly been identified. We have shown that the photochemical association of O and CO to CO_2 may already occur during the relaxation of excited CO in its triplet manifold, and this reaction is definitely complete once CO reaches the lowest triplet state ($a^3\Pi$). Theoretical calculations independently predict the experimental observations correctly. In the DS site O and CO in the complex behave similar to the corresponding isolated species, whereas in the SS site a clear perturbation of the spectroscopic features due to shorter O···CO distance has been observed. In the presence of Xe formation of Xe···O··· CO complexes has been spectroscopically observed in Ar matrices. In Kr matrices, only weak features corresponding to the O···CO complexes could be observed and the spectra were dominated by KrO CT transitions. Probably O atoms escape the mother cage during the photolysis of CO_2 due to much easier mobility of $O(^1D)$ in the Kr lattice. High-level ab initio calculations to get more reliable PES of the O···CO complex correlating to CO_2 in all of the valence excited electronic states, though a difficult task, would give further insight into the energy transfer processes occurring in the O···CO complex, which then could serve as a bench mark for future studies involving photochemically induced energy transfer processes.

Acknowledgment. This work is partly supported by the Deutsche Forschungsgemeinschaft (Project GU 413/3). Travel funds from DESY through BESSY and continuing cooperation of Dr. W. Braun and Dr. G. Reichardt of BESSY are gratefully acknowledged. We thank Mr. Metzner and co-workers at our workshop for excellent maintenance of the apparatus. M.S.G. thanks his wife, Dr. Karin Hassenrück, for financial assistance.

References and Notes

(1) Pringsheim, P. *Fluorescence and Phosphorescence*; Interscience: New York, 1949.
(2) Andrews, D. L. *Chem. Phys.* **1989**, *135*, 195.
(3) Jenkins, R. D.; Andrews, D. L. *Chem. Phys. Lett.* **1999**, *301*, 235.
(4) Andrews, D. L.; Allcock, P. *Chem. Soc. Rev.* **1995**, 259.
(5) Förster, Th. *Discuss. Faraday Soc.* **1959**, *27*, 7.
(6) Gudipati, M. S.; Kalb, M. *Ber. Bunsen-Ges. Phys. Chem.* **1998**, *102*, 249.
(7) Gudipati, M. S.; Kalb, M. *J. Inf. Rec. Mater.* **1998**, *24*, 445.
(8) Harcourt, R. D.; Ghiggino, K. P.; Scholes, G. D.; Speiser, S. *J. Chem. Phys.* **1996**, *105*, 1897.
(9) Dexter, D. L. *J. Chem. Phys.* **1953**, 836.
(10) Scheer, M. D.; Fine, J. *J. Chem. Phys.* **1962**, *36*, 1264.
(11) Slanger, T. G. *J. Chem. Phys.* **1968**, *48*, 586.
(12) Reiland, W.; Tittes, H.-U.; Hertel, I. V.; Bonacic-Koutechky; Persico, M. *J. Chem. Phys.* **1982**, *77*, 1908.
(13) Hammond, G. S.; Saltiel, J. *J. Am. Chem. Soc.* **1963**, *85*, 2515, 2516.
(14) Yamauchi, S.; Azumi, T. *J. Am. Chem. Soc.* **1973**, *95*, 2709.
(15) Vikis, A. C. *Chem. Phys. Lett.* **1975**, *33*, 506.
(16) Vikis, A. C.; Le Roy, D. J. *Chem. Phys. Lett.* **1973**, *22*, 587.
(17) Vikis, A. C.; Le Roy, D. J. *Chem. Phys. Lett.* **1973**, *21*, 103.
(18) Tsuji, M.; Kaneko, N.; Ishimi, H.; Nishimura, Y. *J. Chem. Phys.* **1994**, *101*, 8726.
(19) Harding, D. R.; Weston, R. E., Jr.; Flynn, G. W. *J. Chem. Phys.* **1988**, *88*, 3590.
(20) Matsumi, Y.; Shafer, N.; Tonokura, K.; Kawasaki, M.; Huang, Y.-L.; Gordon, R. J. *J. Chem. Phys.* **1991**, *95*, 7311.
(21) Gudipati, M. S. *J. Phys. Chem. A* **1997**, *101*, 2003.
(22) Klein, A.; Kalb, M.; Gudipati, M. S. *J. Phys. Chem. A* **1999**, *103*, 3843.
(23) Gudipati, M. S.; Kalb, M. *Chem. Phys. Lett.* **1999**, *307*, 27.
(24) Gudipati, M. S.; Kalb, M. *Astron. Astrophys.* **1998**, *329*, 375.
(25) Irvine, M. J.; Mathieson, J. G.; Pullin, A. D. E. *Aust. J. Chem.* **1982**, *35*, 1971.
(26) Dahoo, P. R.; Berrodier, I.; Raducu, V.; Teffo, J. L.; Chabi, H.; Lakhlifi, A.; Abouaf-Marguin, L. *Eur. Phys. J.* **1999**, *D5*, 71.
(27) Bahrdt, J. Doctoral Thesis, Freie Universität Berlin, Berlin, 1987.
(28) Bahrdt, J.; Schwentner, N. *J. Chem. Phys.* **1988**, *88*, 2869.
(29) Effantin, C.; Michaud, F.; Roux, F.; D'Incan, J.; Verges, J. *J. Mol. Spectrosc.* **1982**, *92*, 349.
(30) Gemein, B.; Peyerimhoff, S. D. *Chem. Phys. Lett.* **1991**, *184*, 45.
(31) Fournier, J.; Mohammed, H. H.; Deson, J.; Vermeil, C.; Schamps, J. *J. Chem. Phys.* **1980**, *73*, 6039.
(32) Langhoff, S. R. *J. Chem. Phys.* **1980**, *73*, 2379.
(33) Dunning, T. H., Jr.; Hay, P. J. *J. Chem. Phys.* **1977**, *66*, 3767.
(34) Danilychev, A. V.; Apkarian, V. A. *J. Chem. Phys.* **1994**, *100*, 5556.
(35) Apkarian, V. A.; Schwentner, N. *Chem. Rev.* **1999**, *99*, 1481.
(36) Grünwald, R., Ph.D. Diploma Thesis, University of Hamburg, Hamburg, 1992.
(37) Goodman, J. T. J. C.; Bondybey, V. E.; Brus, L. E. *J. Chem. Phys.* **1977**, *66*, 4802.
(38) Yamanishi, M.; Hirao, K.; Yamashita, K. *J. Chem. Phys.* **1998**, *108*, 1514.
(39) Gudipati, M. S.; Schouren, F.; Kalb. M., to be submitted.
(40) Xantheas, S. S.; Ruedenberg, K. *Int. J. Quantum Chem.* **1994**, *49*, 409.
(41) Abe, M.; Inagaki, Y.; Springsteen, L. L.; Matsumi, Y.; Kawasaki, M.; Tachikawa, H. *J. Phys. Chem.* **1994**, *98*, 12641.
(42) Clyne, M. A. A.; Thrush, B. A. *Proc. R. Soc. London, A* **1962**, *269*, 404.
(43) Frisch, M. J.; Trucks, G. W.; Schlegel, H. B.; Scuseria, G. E.; Robb, M. A.; Cheeseman, J. R.; Zakrzewski, V. G.; Montgomery, J. A., Jr.; Stratmann, R. E.; Burant, J. C.; Dapprich, S.; Millam, J. M.; Daniels, A. D.; Kudin, K. N.; Strain, M. C.; Farkas, O.; Tomasi, J.; Barone, V.; Cossi, M.; Cammi, R.; Mennucci, B.; Pomelli, C.; Adamo, C.; Clifford, S.; Ochterski, J.; Petersson, G. A.; Ayala, P. Y.; Cui, Q.; Morokuma, K.; Malick, D. K.; Rabuck, A. D.; Raghavachari, K.; Foresman, J. B.; Cioslowski, J.; Ortiz, J. V.; Stefanov, B. B.; Liu, G.; Liashenko, A.; Piskorz, P.; Komaromi, I.; Gomperts, R.; Martin, R. L.; Fox, D. J.; Keith, T.; Al-Laham, M. A.; Peng, C. Y.; Nanayakkara, A.; Gonzalez, C.; Challacombe, M.; Gill, P. M. W.; Johnson, B. G.; Chen, W.; Wong, M. W.; Andres, J. L.; Head-Gordon, M.; Replogle, E. S.; Pople, J. A. *Gaussian 98*; Gaussian, Inc.: Pittsburgh, PA, 1998.
(44) Manz, J.; Mirsky, K. *Chem. Phys.* **1980**, *46*, 457.
(45) Mirsky, K. *Chem. Phys.* **1980**, *46*, 445.
(46) Sevryuk, M. B.; Billing, G. D. *Chem. Phys.* **1994**, *185*, 199.
(47) Winter, M.; Seranski, K.; Schurath, U. *Chem. Phys.* **1992**, *159*, 235.
(48) Press, W. H.; Teukolsky, S. A.; Vetterling, W. T.; Flannery, B. P. *Numerical Recipes*; Cambridge University Press: Cambridge, 1988.